

# Magnetic Field Distribution of an Elliptical Permanent Magnet

Van Tai Nguyen<sup>1, 2, \*</sup>, Tien-Fu Lu<sup>1</sup>, Will Robertson<sup>1</sup>, and Paul Grimshaw<sup>1</sup>

**Abstract**—The magnetic field distribution of an axially magnetised cylinder with an elliptical profile is analytically modelled and analysed in this paper. An accurate and fast-computed semi-analytical model is developed, based on the charge model and geometrical analysis, to compute three components of the magnetic field generated by this elliptical cylinder in three-dimensional space. The accuracy of the model is verified using Finite Element Analysis. The analytical expressions are efficient for calculating the implementation of the magnetic field, taking less than one millisecond to execute on a modern PC. Using the fast-computed analytical model, the distribution of the magnetic field of an axially magnetised cylinder with different elliptical profiles is studied and compared with that of a circular cylinder. The variations in magnetic field strength of axial, azimuthal and radial components can be used in novel sensing applications. The derived analytical model can be extended to calculate the magnetic field of arc-shaped elliptical and circular cylinders with axial magnetization, which can be used in Halbach arrangements.

## 1. INTRODUCTION

Understanding magnetic field distribution of a permanent magnet plays a key role in developing magnetic sensing devices [1] and medical appliances (i.e., magnetic resonance imaging) [2]. In other applications such as magnetic suspensions, levitated magnetic disks, magnetic gears, and magnetic couplings, the forces and torques generated by permanent magnets are of great interest [3]. These forces ( $\vec{F}$ ) and torques ( $\vec{T}$ ) can be computed using the charge model, involving the magnetic field [4] as:

$$\vec{F} = \iiint_v \vec{B}_{ext} \sigma_{mv} dv + \iint_s \vec{B}_{ext} \sigma_{ms} ds$$

and

$$\vec{T} = \iiint_v (\vec{r} \times \vec{B}_{ext}) \sigma_{mv} dv + \iint_s (\vec{r} \times \vec{B}_{ext}) \sigma_{ms} ds$$

where  $\vec{B}_{ext}$  is the external magnetic field;  $\sigma_{mv}$  is the volume charge of a given magnet with a magnetization vector  $\vec{J}$ ;  $\sigma_{mv} = -\vec{\nabla} \cdot \vec{J}$ ;  $\sigma_{ms}$  is the surface charge of the given magnet;  $\sigma_{ms} = \vec{J} \cdot \vec{n}$ ;  $\vec{n}$  is the normal vector to the impacted surface of the given magnet;  $\vec{r}$  is the distance between the magnetic field source and the given magnet; and  $V$  and  $S$  denote the volume and surface area of the given magnet, respectively. A fast-computed model of the magnetic field source generated by a permanent magnet is important to facilitate the design, optimization, and dynamical modelling of devices and systems using permanent magnets.

Although magnetic field solutions for generalized geometries are available using Finite Element Analysis (FEA), and this method is inefficient for 3D problems, with a substantial tradeoff between computation time and accuracy. To address this issue, magnetic field solutions of permanent magnets

---

Received 16 August 2019, Accepted 19 November 2019, Scheduled 28 November 2019

\* Corresponding author: Van Tai Nguyen (tainv@tlu.edu.vn or vantai.nguyen@adelaide.edu.au).

<sup>1</sup> School of Mechanical Engineering, University of Adelaide, SA 5005, Australia. <sup>2</sup> Faculty of Mechanical Engineering, Thuyloi University, 175 Tay Son, Dong Da, Hanoi, Vietnam.

with specific shapes and configurations have been analytically modelled and studied [3–15]. Ravaud et al. [4] developed analytical models to calculate the magnetic field of ring-shaped permanent magnets with axial and radial magnetization. Xu et al. [5] studied the strong magnetic field of a permanent magnet array used in refrigeration. Ravaud et al. [6] derived the exact analytical model to compute the magnetic field produced by a radially magnetized tile permanent magnet. Jian and Chan [7] analytically calculated the magnetic field distribution of magnetic gears. Yonnet et al. [8] derived an analytical model to calculate permanent magnet couplings. McClurg [9] studied the magnetic field distribution of a sphere and ellipsoid. Based on a Coulombian approach, Rakotoarison et al. [10] modelled the scalar potential and magnetic field of an arc-shaped permanent magnet with radial magnetization. Nguyen and Lu [11] derived an analytical model to calculate the magnetic field of a circular cylinder with diametrical magnetization. Ravaud and Lemarquand [12] analysed the magnetic field of a parallelepipedic magnet. Nguyen and Lu [13] developed a fast-computed model to study the magnetic field distribution of an elliptical cylinder with diametrical magnetization. However, the distribution of the magnetic field of an elliptical cylinder with axial magnetization has not been analytically expressed and studied in the literature.

Inspired by the fact that elliptical profiles have been widely found in physics, astronomy, and engineering [13]. For example, the orbit of each planet in the solar system is approximately an ellipse [16]. Elliptical gears have been found to acquire great efficiency in motion and power transmission solutions [17–19]; hence, the magnetic field distribution and application of a permanent magnet with elliptical profiles could be of great interest [9]. Moreover, a fast-computed model to calculate the magnetic field could facilitate the design process of an elliptical permanent magnet used for surface magnetic resonance imaging [20], a novel magnetic coupler [21], the design of permanent magnetic gears [7], and couplings [8] with elliptical profiles as well as a non-contact cam mechanism [22] using an axially magnetised driver with an elliptical profile. Furthermore, for educational purposes, this research would assist students in understanding the magnetic field distribution of the elliptical cylinder permanent magnet as an example beyond the common permanent magnets in cuboid, ring, and circular cylindrical shapes, which are commonly found in textbooks [3]. In addition, having in hand a model of the magnetic field of an elliptical cylinder with axial and diametrical magnetizations, the distribution of the magnetic field of an elliptical cylinder with arbitrarily uniform magnetization, which is a combination of the axial and diametrical magnetizations [23], can be predicted, thanks to the superposition principle.

These motivations led to the modelling and study of the magnetic field distribution of an elliptical cylinder with uniformly axial magnetization in this paper. The charge model [3] and geometric analyses are applied to derive the semi-analytical expressions of the axial, azimuthal, and radial components of the magnetic field created by the cylinder in three-dimensional (3D) space. FEA was conducted to verify the accuracy of the analytical model, and the efficiency of these expressions was also demonstrated. Furthermore, the fast-computed analytical model makes it possible to study the distribution of the magnetic field created by an axially magnetized cylinder with different elliptical profiles and compare it with that of a circular cylinder.

This paper is organized as follows. Section 2 describes the mathematical formulation of the analytical model. Section 3 presents the Finite Element verification. Section 4 discusses the distribution of the magnetic field of a cylinder with different elliptical profiles. Section 5 draws the conclusion.

## 2. MATHEMATICAL FORMULATION

The geometry of an elliptical cylinder used to derive expressions of the three magnetic field components is illustrated in Figure 1 and Figure 2. It is assumed that the magnetization  $\vec{J}$  is uniformly distributed along axis  $Z$ , as depicted in Figure 1(a), and the thickness of the cylinder is  $h$ . The elliptical profile of the cylinder is presented in Figure 2; here,  $F_1$  and  $F_2$  are the foci of the ellipse;  $a$  is the length of the semi-major axis; and  $b$  is the length of the semi-minor axis. The general equation for the ellipse Eq. (1) has a parametric representation using sine and cosine functions as  $\vec{V} = (x, y) = (a \cos \tau, b \sin \tau)$ ,  $0 \leq \tau < 2\pi$ ;  $\tau$  can be defined as shown in Figure 2, based on de la Hire [24], where  $A$  is on a circle with a radius of  $a$ , and  $B$  is on a circle with a radius of  $b$ .

$$\frac{x^2}{a^2} + \frac{y^2}{b^2} = 1 \quad (1)$$

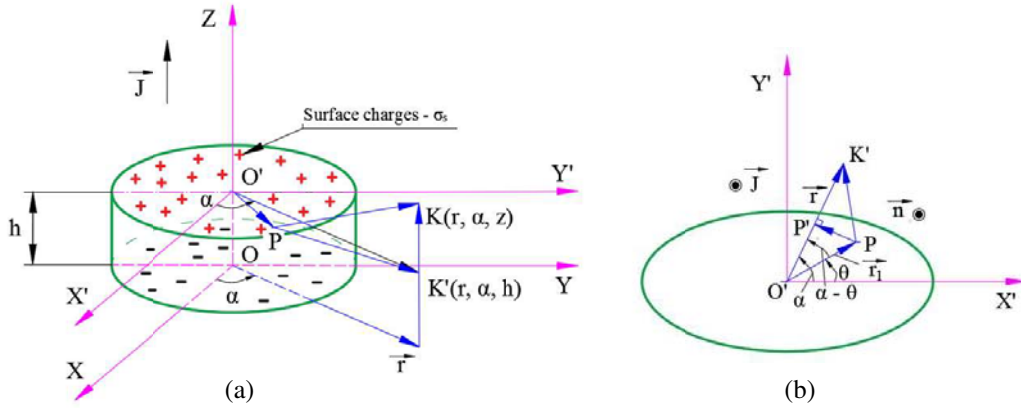


**Figure 1.** Computed elliptical cylinder: (a) 3D model of the elliptical cylinder; (b) Projection of the cylinder on an  $O'X'Y'$  plane.

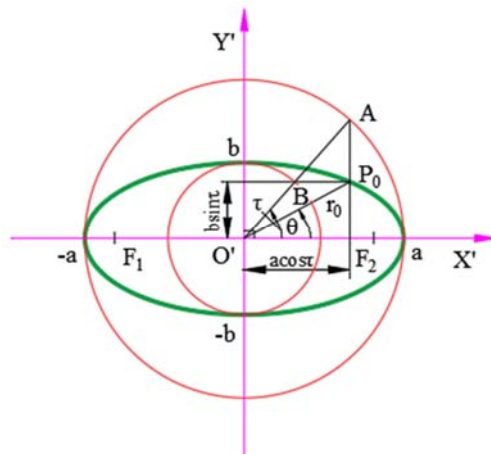


**Figure 2.** Schematic of the elliptical profile of the cylinder [24].

Under static conditions, the well-known governing equations which are so-called Maxwell equations (Eqs. (M.1)–(M.4)) for electromagnetism can be presented as follows:

$$\vec{\nabla} \times \vec{H} = \vec{j} \tag{M.1}$$

$$\vec{\nabla} \cdot \vec{B} = 0 \tag{M.2}$$

$$\vec{\nabla} \times \vec{E} = 0 \tag{M.3}$$

$$\vec{\nabla} \cdot \vec{D} = \rho \tag{M.4}$$

and the constitutive equations linking  $\vec{B}$  to  $\vec{H}$  and  $\vec{D}$  to  $\vec{E}$  are expressed as  $\vec{B} = \mu_0 \vec{H} + \vec{J}$  (M.5) and  $\vec{D} = \epsilon_0 \vec{E}$  (M.6), respectively.

Here,  $j$  ( $A/m^2$ ) and  $\rho$  ( $C/m^3$ ) are the electric current density and electric charge density, respectively;  $E$  is the electric field intensity ( $V/m$ );  $D$  is the electric flux density ( $C/m^2$ );  $H$  is the magnetic field intensity ( $A/m$ );  $B$  is the magnetic flux density ( $T$ );  $\mu_0$  ( $H/m$ ) and  $\epsilon_0$  ( $F/m$ ) are the permeability and permittivity of the vacuum, respectively;  $J(T)$  is the intensity of magnetization.

By introducing the surface charge density  $\sigma_s$  and the volume charge density  $\sigma_v$  with some simplifications, these equations (Eqs. (M.1)–(M.6)) can be turned into a new form which is called the charge model (the derivation steps can be found in the work of Furlani [3].) to calculate the magnetic field created by a permanent magnet in three-dimensional free space. Based on this charge model, the

magnetic field intensity  $\vec{H}_K$  at any point  $K(r, \alpha, z)$  in a cylindrical coordinate system can be computed using Eq. (2).

$$\vec{H}_K = \frac{1}{4\pi\mu_0} \left( \iint_s \frac{\sigma_s}{|\vec{PK}|^3} \vec{PK} ds + \iiint_v \frac{\sigma_v}{|\vec{PK}|^3} \vec{PK} dv \right) \quad (2)$$

where  $P$  is a point on the surface of the cylinder (Figure 1(a));  $v$  and  $s$  denote the volume and surface area of the given magnet, respectively.

The volume charge density  $\sigma_v$  in Eq. (2) can be calculated as follows:

$$\sigma_v = -\vec{\nabla} \cdot \vec{J} \quad (3)$$

Since the magnetisation vector  $\vec{J}$  is uniformly axial, and its divergence is equal to zero, which means  $\sigma_v = 0$ . This means that the volume charge has no contribution to the magnetic field; hence, the magnetic field intensity  $\vec{H}_K$  at point  $K$  can be calculated using only the surface charge:

$$\vec{H}_K = \frac{1}{4\pi\mu_0} \iint_s \frac{\sigma_s}{|\vec{PK}|^3} \vec{PK} ds \quad (4)$$

where the surface charge density  $\sigma_s$  can be calculated as follows:

$$\sigma_s = \vec{J} \cdot \vec{n} = \begin{cases} J & \text{for the upper surface} \\ 0 & \text{for the cylindrical surface} \\ -J & \text{for the lower surface} \end{cases} \quad (5)$$

Here,  $\vec{n}$  is the unit vector normal to the surface, for the top and bottom bases of the cylinder, and  $\vec{n}$  is parallel to vector  $\vec{J}$  and perpendicular to  $\vec{J}$  for the cylindrical surface. Thus, only the upper and lower surfaces of the cylinder contribute to the magnetic field.

From Eqs. (4) and (5), the magnetic field in a cylindrical coordinate system  $(r, \alpha, z)$  with azimuth coincident with axis  $X$  is:

$$\begin{aligned} \vec{H}_{K(r,\alpha,z)} &= \vec{H}_{K(r,\alpha,z)}^+ + \vec{H}_{K(r,\alpha,z)}^- \\ &= \frac{J}{4\pi\mu_0} \int_{\theta=-\pi}^{\theta=\pi} \int_{r_1=0}^{r_1=r_0} \frac{\vec{PK}^+}{|\vec{PK}^+|^3} r_1 dr_1 d\theta + \frac{-J}{4\pi\mu_0} \int_{\theta=-\pi}^{\theta=\pi} \int_{r_1=0}^{r_1=r_0} \frac{\vec{PK}^-}{|\vec{PK}^-|^3} r_1 dr_1 d\theta \end{aligned} \quad (6)$$

where the sign “+” refers to the magnetic field from the upper surface, and “-” refers to the lower surface.

From Figure 2,

$$r_0 = O'P_0 = \sqrt{a^2 \cos^2 \tau + b^2 \sin^2 \tau} \quad (7)$$

and

$$a \cos \tau = O'P_0 \cos \theta \quad (8)$$

$$b \sin \tau = O'P_0 \sin \theta \quad (9)$$

Dividing Eq. (8) by (9), we achieve:

$$\frac{a}{b} \cot \tau = \cot \theta \quad (10)$$

Inserting Eq. (10) into Eq. (7) produces:

$$r_0 = \frac{ab}{\sqrt{a^2 \sin^2 \theta + b^2 \cos^2 \theta}} \quad (11)$$

Firstly, we compute the magnetic field created by the upper surface.

From Figures 1(a) and 1(b), the vector  $\vec{PK}^+$  can be projected on the radial, azimuthal, and axial directions ( $\vec{u}_r$ ,  $\vec{u}_\alpha$ , and  $\vec{u}_z$  are the unit vectors respectively) as follows:

$$\vec{PK}^+ = \overline{PP'}^+ + \overline{P'K'}^+ + \overline{K'K}^+ = r_1 \sin(\alpha - \theta) \vec{u}_\alpha + (r - r_1 \cos(\alpha - \theta)) \vec{u}_r + (z - h) \vec{u}_z \quad (12)$$

Inserting Eq. (12) into Eq. (6) gives:

$$\vec{H}_{K(r,\alpha,z)}^+ = \frac{J}{4\pi\mu_0} \int_{\theta=-\pi}^{\theta=\pi} \int_{r_1=0}^{r_1=r_0} \frac{r_1 \sin(\alpha - \theta) \vec{u}_\alpha + (r - r_1 \cos(\alpha - \theta)) \vec{u}_r + (z - h) \vec{u}_z}{\left(r_1^2 + r^2 - 2r_1 r \cos(\alpha - \theta) + (z - h)^2\right)^{\frac{3}{2}}} r_1 dr_1 d\theta \quad (13)$$

The axial, azimuthal, and radial components of the magnetic field can be derived from Eq. (13), as detailed in the following sections.

### 2.1. The Axial Component $H_{K(z)}^{(3D)}(r, \alpha, z)$

The axial component is expressed as the superposition of the contribution of two faces:  $H_{K(z)}^{(3D)}(r, \alpha, z) = H_{K(z)}^{(3D)+}(r, \alpha, z) + H_{K(z)}^{(3D)-}(r, \alpha, z)$ . From Eq. (13),  $H_{K(z)}^{(3D)+}(r, \alpha, z)$  can be expressed as follows:

$$H_{K(z)}^{(3D)+}(r, \alpha, z) = \frac{J}{4\pi\mu_0} \int_{\theta=-\pi}^{\theta=\pi} \int_{r_1=0}^{r_1=r_0} \frac{(z - h)}{\left(r_1^2 + r^2 - 2r_1 r \cos(\alpha - \theta) + (z - h)^2\right)^{\frac{3}{2}}} r_1 dr_1 d\theta \quad (14)$$

Integrating Eq. (14) based on  $r_1$  with some simplifications yields (Appendix A):

$$H_{K(z)}^{(3D)+}(r, \alpha, z) = \frac{J}{4\pi\mu_0} \int_{\theta=-\pi}^{\theta=\pi} \left( \frac{2(\delta r_0 - 2\xi_+)}{(4\xi_+ - \delta^2) \sqrt{r_0(r_0 - \delta) + \xi_+}} + \frac{4\sqrt{\xi_+}}{4\xi_+ - \delta^2} \right) (z - h) d\theta \quad (15)$$

where  $\delta = 2r \cos(\alpha - \theta)$  and  $\xi_+ = r^2 + (z - h)^2$ .

It is noted that  $4\xi_+ - \delta^2 = 4r^2 + 4(z - h)^2 - 4r^2 \cos^2(\alpha - \theta) > 0$  except the singularity case when  $z = h$  and  $\alpha - \theta = l\pi; l = 0, 1, 2, 3, \dots$ . This singularity can be easily removed when executing Eq. (15) to avoid indefinite result.

The contribution of the lower surface can be derived, following the same steps as above to achieve, with  $\xi_- = r^2 + z^2$ . Similar to the above notation,  $4\xi_- - \delta^2 = 4r^2 + 4z^2 - 4r^2 \cos^2(\alpha - \theta) > 0$  except the singularity case when  $z = 0$  and  $\alpha - \theta = l\pi; l = 0, 1, 2, 3, \dots$

$$H_{K(z)}^{(3D)-}(r, \alpha, z) = \frac{-J}{4\pi\mu_0} \int_{\theta=-\pi}^{\theta=\pi} \left( \frac{2(\delta r_0 - 2\xi_-)}{(4\xi_- - \delta^2) \sqrt{r_0(r_0 - \delta) + \xi_-}} + \frac{4\sqrt{\xi_-}}{4\xi_- - \delta^2} \right) (z) d\theta \quad (16)$$

### 2.2. The Tangential (Azimuthal) Component $H_{K(\alpha)}^{(3D)}(r, \alpha, z)$

The azimuthal component  $H_{K(\alpha)}^{(3D)}(r, \alpha, z) = H_{K(\alpha)}^{(3D)+}(r, \alpha, z) + H_{K(\alpha)}^{(3D)-}(r, \alpha, z)$ . From Eq. (13),  $H_{K(\alpha)}^{(3D)+}(r, \alpha, z)$  can be expressed as follows:

$$H_{K(\alpha)}^{(3D)+}(r, \alpha, z) = \frac{J}{4\pi\mu_0} \int_{\theta=-\pi}^{\theta=\pi} \int_{r_1=0}^{r_1=r_0} \frac{r_1^2 \sin(\alpha - \theta)}{\left(r_1^2 + r^2 - 2r_1 r \cos(\alpha - \theta) + (z - h)^2\right)^{\frac{3}{2}}} dr_1 d\theta \quad (17)$$

Integrating Eq. (17) based on  $r_1$  with some simplifications produces (Appendix A):

$$H_{K(\alpha)}^{(3D)+}(r, \alpha, z) = \frac{J}{4\pi\mu_0} \int_{\theta=-\pi}^{\theta=\pi} \left( \ln \left( 2 \left( \sqrt{r_0(r_0 - \delta) + \xi_+} + r_0 \right) - \delta \right) - \frac{2(2\xi_+ - \delta^2)r_0 + 2\delta\xi_+}{(4\xi_+ - \delta^2) \sqrt{r_0(r_0 - \delta) + \xi_+}} \right. \\ \left. - \ln(2\sqrt{\xi_+} - \delta) + \frac{2\delta\xi_+}{(4\xi_+ - \delta^2) \sqrt{\xi_+}} \right) \sin(\alpha - \theta) d\theta \quad (18)$$

The contribution of the lower surface can be derived, following the same steps as above to achieve:

$$H_{K(\alpha)}^{(3D)-}(r, \alpha, z) = \frac{-J}{4\pi\mu_0} \int_{\theta=-\pi}^{\theta=\pi} \left( \ln \left( 2 \left( \sqrt{r_0(r_0-\delta)} + \xi_- + r_0 \right) - \delta \right) - \frac{2(2\xi_- - \delta^2)r_0 + 2\delta\xi_-}{(4\xi_- - \delta^2)\sqrt{r_0(r_0-\delta)} + \xi_-} \right. \\ \left. - \ln(2(\sqrt{\xi_-}) - \delta) + \frac{2\delta\xi_-}{(4\xi_- - \delta^2)\sqrt{\xi_-}} \right) \sin(\alpha - \theta) d\theta \quad (19)$$

### 2.3. The Radial Component $H_{K(r)}^{(3D)}(r, \alpha, z)$

The radial component  $H_{K(r)}^{(3D)}(r, \alpha, z) = H_{K(r)}^{(3D)+}(r, \alpha, z) + H_{K(r)}^{(3D)-}(r, \alpha, z)$ . From Eq. (13),  $H_{K(r)}^{(3D)}(r, \alpha, z)$  can be expressed as follows:

$$H_{K(r)}^{(3D)}(r, \alpha, z) = \frac{J}{4\pi\mu_0} \int_{\theta=-\pi}^{\theta=\pi} \int_{r_1=0}^{r_1=r_0} \frac{(r - r_1 \cos(\alpha - \theta))}{\left( r_1^2 + r^2 - 2r_1r \cos(\alpha - \theta) + (z - h)^2 \right)^{\frac{3}{2}}} r_1 dr_1 d\theta \quad (20)$$

Integrating Eq. (20) based on  $r_1$  with  $\Upsilon = \cos(\alpha - \theta)$  with some simplifications gives (Appendix A):

$$H_{K(r)}^{(3D)+}(r, \alpha, z) = \frac{J}{4\pi\mu_0} \int_{\theta=-\pi}^{\theta=\pi} \left( \frac{2(\delta r + 2\xi_+ \Upsilon - \delta^2 \Upsilon)r_0 - 4\xi_+ r + 2\delta\xi_+ \Upsilon}{(4\xi_+ - \delta^2)\sqrt{r_0(r_0-\delta)} + \xi_+} \right. \\ \left. - \Upsilon \ln \left( 2 \left( \sqrt{r_0(r_0-\delta)} + \xi_+ + r_0 \right) - \delta \right) - \frac{-4\xi_+ r + 2\delta\xi_+ \Upsilon}{(4\xi_+ - \delta^2)\sqrt{\xi_+}} + \Upsilon \ln(2\sqrt{\xi_+} - \delta) \right) d\theta \quad (21)$$

The contribution of the lower surface can be derived, following the same steps as above to achieve:

$$H_{K(r)}^{(3D)-}(r, \alpha, z) = \frac{-J}{4\pi\mu_0} \int_{\theta=-\pi}^{\theta=\pi} \left( \frac{2(\delta r + 2\xi_- \Upsilon - \delta^2 \Upsilon)r_0 - 4\xi_- r + 2\delta\xi_- \Upsilon}{(4\xi_- - \delta^2)\sqrt{r_0(r_0-\delta)} + \xi_-} \right. \\ \left. - \Upsilon \ln \left( 2 \left( \sqrt{r_0(r_0-\delta)} + \xi_- + r_0 \right) - \delta \right) - \frac{-4\xi_- r + 2\delta\xi_- \Upsilon}{(4\xi_- - \delta^2)\sqrt{\xi_-}} + \Upsilon \ln(2\sqrt{\xi_-} - \delta) \right) d\theta \quad (22)$$

From the magnetic field intensity  $\vec{H}_K$ , the magnetic flux density  $\vec{B}_K$  can be computed with:

$$\vec{B}_K = \mu_0 \vec{H}_K \quad (\text{in the air space}) \quad (23)$$

$$\vec{B}_K = \mu_0 \vec{H}_K + \vec{J} \quad (\text{inside the magnet}) \quad (24)$$

In the case where  $a = b$ , the elliptical cylinder is simplified to a circular cylinder; hence the derived expressions could also be implemented to calculate the magnetic field generated by a circular cylinder permanent magnet with uniformly axial magnetization.

Following the same derivation steps as presented above, the magnetic field created by an arc-shaped elliptical cylinder (which is aligned with the Cartesian and cylindrical coordinate systems as presented in Figure 3) with uniformly axial magnetization can be computed using the derived expressions for the three components with an integral interval of  $\theta$  from 0 to the arc angle  $\gamma$  instead of  $[-\pi, \pi]$ . The calculation of magnetic field of this arc-shaped cylinder can facilitate the design and optimization of a Hallbach permanent magnet [25] which may include pieces of permanent magnet of this kind.

## 3. FINITE ELEMENT VERIFICATION

Finite Element Analysis (FEA) is a commonly used method to study problems in various fields. In static electromagnetism, this method aims at solving the governing and constitutive equations listed in Section 2 (Eqs. (M.1)–(M.6)). In this research, FEA is implemented to verify the accuracy of the semi-analytical model using Electromagnetic Simulation Software®(EMS) (EMWorks, Inc., Montreal, Quebec, Canada). The parameters of the used elliptical cylinder made of rare earth material (Figure 2) are:  $a = 6$  mm,  $b = 3$  mm,  $h = 5$  mm, and magnetization  $J = 1$  T which is axially oriented.

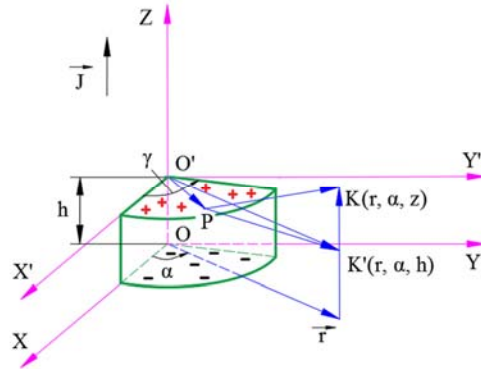


Figure 3. Arc-shaped elliptical cylinder.

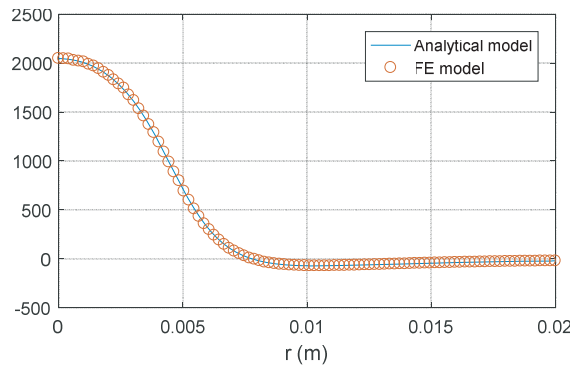


Figure 4. FEA verification results for axial component (the parameters of the used elliptical cylinder (Figure 2) are:  $a = 0.006$  m,  $b = 0.003$  m,  $h = 0.005$  m,  $J = 1$  T); plots along the radial distance with  $z = 0.007$  m and  $r$  from 0 m to 0.020 m.

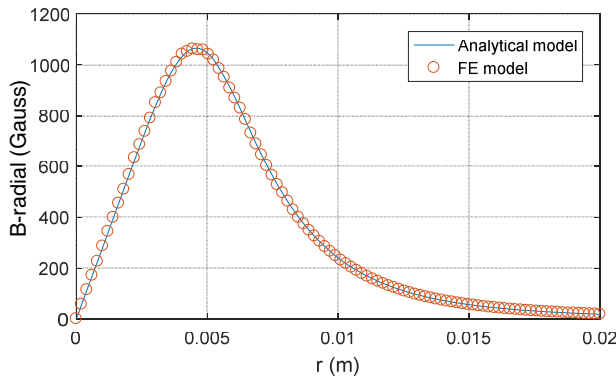


Figure 5. FEA verification results for radial component (the parameters of the used elliptical cylinder (Figure 2) are:  $a = 0.006$  m,  $b = 0.003$  m,  $h = 0.005$  m,  $J = 1$  T); plots along the radial distance with  $z = 0.007$  m and  $r$  from 0 m to 0.020 m.

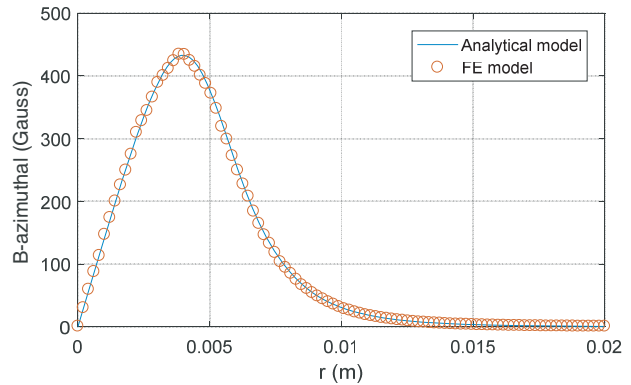


Figure 6. FEA verification results for azimuthal component (the parameters of the used elliptical cylinder (Figure 2) are:  $a = 0.006$  m,  $b = 0.003$  m,  $h = 0.005$  m,  $J = 1$  T); plots along the radial distance with  $z = 0.007$  m and  $r$  from 0 m to 0.020 m.

The plots of three components of the magnetic field generated by the given elliptical cylinder are illustrated in Figures 4, 5, and 6. Three components of magnetic field of ten points with random  $r$  (mm) are extracted from these figures and listed in Table 1 including the errors of computed results using the derived analytical model against those of Finite Element Analysis.

**Table 1.** Analytical results vs FEA results for 10 points with random  $r$  (mm) and errors of results between two methods (Max — Maximum; Aver — Average; Min — Minimum).

Points ( $r$ mm, 30°, 7 mm)	Axial component (Gauss)			Azimuthal component (Gauss)			Radial component (Gauss)		
	Analytical results	FEA results		Analytical results	FEA results		Analytical results	FEA results	
1.01	2004.985	2012.765		142.500	147.123		282.559	286.766	
2.22	1828.209	1829.148		302.959	309.872		623.767	633.473	
3.43	1457.334	1457.554		417.049	411.765		931.164	933.559	
5.25	599.604	596.804		350.571	348.170		1019.055	1018.313	
6.67	145.592	144.049		185.266	184.216		733.565	730.477	
8.89	-58.102	-58.166		54.862	54.466		348.896	348.724	
13.13	-59.326	-59.374		7.207	7.217		92.435	92.307	
17.17	-34.112	-34.081		1.579	1.563		33.517	33.484	
18.18	-29.717	-29.686		1.135	1.133		26.859	26.834	
19.79	-24.015	-23.986		0.693	0.687		19.289	19.223	
Error (%)	Max	Aver	Min	Max	Aver	Min	Max	Aver	Min
	1.07	0.25	0.015	3.14	1.08	0.13	1.53	0.45	0.049

It can be seen from Table 1 and Figures 4, 5, and 6 that the results of the magnetic field computed using the derived semi-analytical model are in excellent agreement with those computed using the FEA model (the average errors between two models are 0.25% for axial component, 1.08% for azimuthal component, and 0.45% for radial component (Table 1)).

Evaluated in MATLAB R2016b (MathWorks, Natick, MA, USA), it took an average of 0.75 ms on a personal computer (Intel Core i7-6700 CPU, 3.40 GHz) to calculate each component, using the derived expressions at a single location (2000 samplepoints were used in this evaluation), whereas on the other hand, it could take up to several hours with small scale of mesh (the smaller the mesh is, the more computation time it consumes) to complete the simulation using FEA on the same personal computer.

#### 4. ANALYSIS OF THE MAGNETIC FIELD DISTRIBUTION

In this section, the magnetic field distribution created by an axially magnetized cylinder with different elliptical profiles is plotted along the radial distance  $r$  in the interval  $[0 \text{ mm}, 20 \text{ mm}]$  with the azimuthal angle  $\alpha = \pi/6$ , and along the azimuthal angle  $\alpha$  (alpha) in the interval of  $[-\pi, \pi]$  with the radial distance  $r = 8 \text{ mm}$ . The thickness of the used cylinder is  $h = 5 \text{ mm}$ ; the magnetic remanence  $J = 1 \text{ T}$ ; the axial coordinate of the computed profile is  $z = 7 \text{ mm}$ ; the elliptical profiles of the cylinder vary due to the

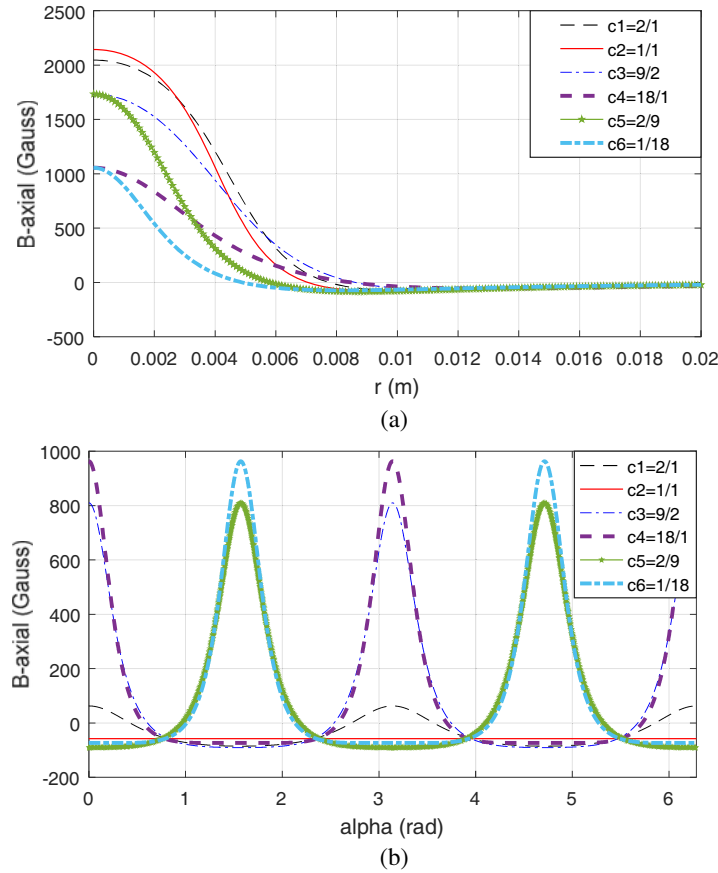


**Figure 7.** Distribution of the axial component (the thickness of the used cylinder is  $h = 5$  mm; the magnetic remanence  $J = 1$  T; the axial coordinate of the computed profile is  $z = 7$  mm): (a) plot along the radial distance in the interval  $[0 \text{ mm}, 20 \text{ mm}]$  with azimuthal angle  $\alpha = \pi/6$ ; (b) plot along the azimuthal angle  $\alpha$  (alpha) with radial distance  $r = 8$  mm.

changes in the so-called axis ratio  $c$  of the major semi-axis  $a$  and semi-minor axis  $b$ ,  $c = a/b$ . The plots of the magnetic field distribution were carried out in six cases:  $c1 = 6/3 = 2/1$ ;  $c2 = \sqrt{18}/\sqrt{18} = 1/1$ ;  $c3 = 9/2$ ;  $c4 = 18/1$ ;  $c5 = 2/9$  and  $c6 = 1/18$ . It is noted here that regardless of the variations in profiles, the ellipses have the same area  $S = \pi ab = 18\pi \text{ mm}^2$ .

Figure 7(a) shows that the amplitude of the axial component of a circular cylinder ( $c2 = 1/1$ ) is the largest (2143 Gauss) at the beginning  $r = 0$  mm, and it eventually drops down to below those of  $c1$  (from  $r = 2.8$  mm),  $c3$  (from  $r = 4.5$  mm) and  $c4$  (from  $r = 6.1$  mm). All the other amplitudes decrease when  $r$  increases. Figure 7(b) demonstrates that the magnetic field of a circular cylinder ( $c2 = 1/1$ ) is a negative constant ( $-57.64$  Gauss) along the azimuthal angle (Table 2), whereas the magnetic field distribution of an elliptical cylinder is periodic and obtains both positive and negative values; the amplitudes of the periodical distribution (Table 2) are 62.69 Gauss for  $c1$ , 810.0 Gauss for  $c3$ , 963.1 Gauss for  $c4$ , 810.0 Gauss for  $c5$ , and 963.2 Gauss for  $c6$ . It can be concluded that, for the same area, the elliptical cylinder, compared with the circular cylinder, has the interesting properties of producing larger magnetic field amplitudes and periodical distributions of the magnetic field.

Figures 8(a) and 8(b) show that the azimuthal distribution of the magnetic field of a circular cylinder is zero (Table 2) due to its symmetry. However, elliptical cylinders can yield large amplitudes, which vary according to changes of the axis ratio  $c$ . The magnetic field distribution along the radial distance  $r$  can obtain both negative and positive values; their maximum amplitudes are 432.9 Gauss at  $r = 4$  mm for  $c1$ , 683.8 Gauss at  $r = 4$  mm for  $c3$ , 522.2 Gauss at  $r = 3.8$  mm for  $c4$ ,  $-433.8$  Gauss at  $r = 2.7$  mm for  $c5$  and  $-306.1$  Gauss at  $r = 2.3$  mm for  $c6$ . The magnetic field distribution of the

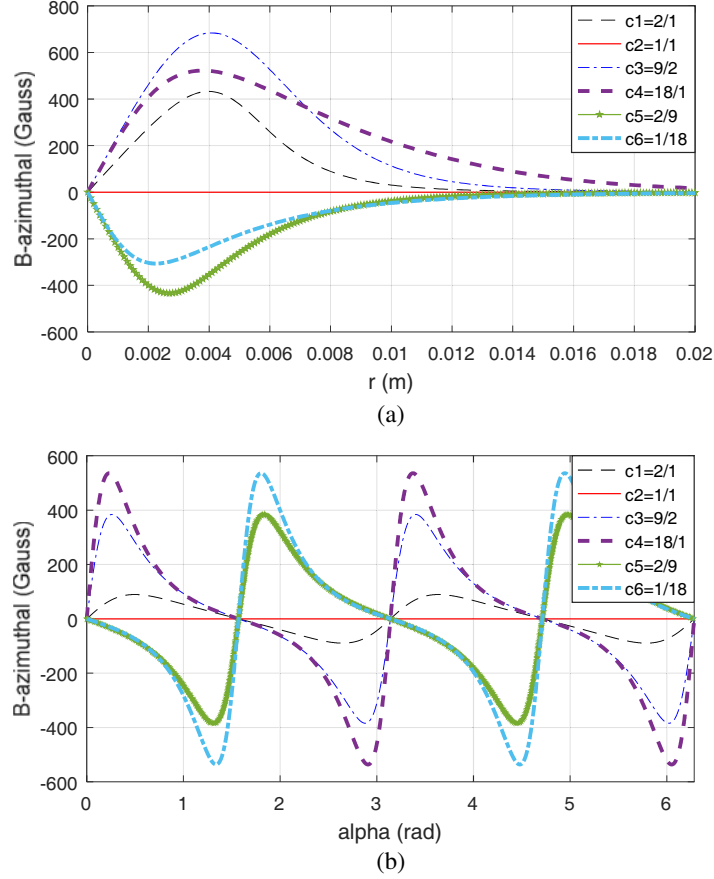


**Figure 8.** Distribution of the azimuthal component (the thickness of the used cylinder is  $h = 5$  mm; the magnetic remanence  $J = 1$  T; the axial coordinate of the computed profile is  $z = 7$  mm): (a) plot along the radial distance  $r$  in the interval  $[0 \text{ mm}, 20 \text{ mm}]$  with azimuthal angle  $\alpha = \pi/6$ ; (b) plot along the azimuthal angle  $\alpha$  (alpha) with radial distance  $r = 8$  mm.

**Table 2.** Amplitudes of the periodical distribution of magnetic field.

Axis ratio $c = a/b$	Axial component (Gauss)	Azimuthal component (Gauss)	Radial component (Gauss)
$c1 = 2/1$	62.69	89.45	594.0
$c2 = 1/1$	-57.64	0	411.7
$c3 = 9/2$	810.0	384.2	756.2
$c4 = 18/1$	963.1	536.0	248.6
$c5 = 2/9$	810.0	384.2	756.2
$c6 = 1/18$	963.2	536.0	248.6

azimuthal component (Table 2) is periodical along the azimuthal angle (Figure 8(b)); the amplitudes of this distribution are 89.45 Gauss for  $c1$ , 384.2 Gauss for  $c3$ , 536.0 Gauss for  $c4$ , 384.2 Gauss for  $c5$ , and 536.0 Gauss for  $c6$ .

In contrast with the distribution of axial and azimuthal components, the radial component of the field consists of only positive values (Figures 9(a) and 9(b)). The amplitudes of the radial component of a circular and an elliptical cylinder vary according to the changes of  $r$ ; the maximum amplitudes are 1065 Gauss at  $r = 4.6$  mm for  $c1$ , 1224 Gauss at  $r = 4.1$  mm for  $c2$ , 725.4 Gauss at  $r = 4.8$  mm for  $c3$ ,

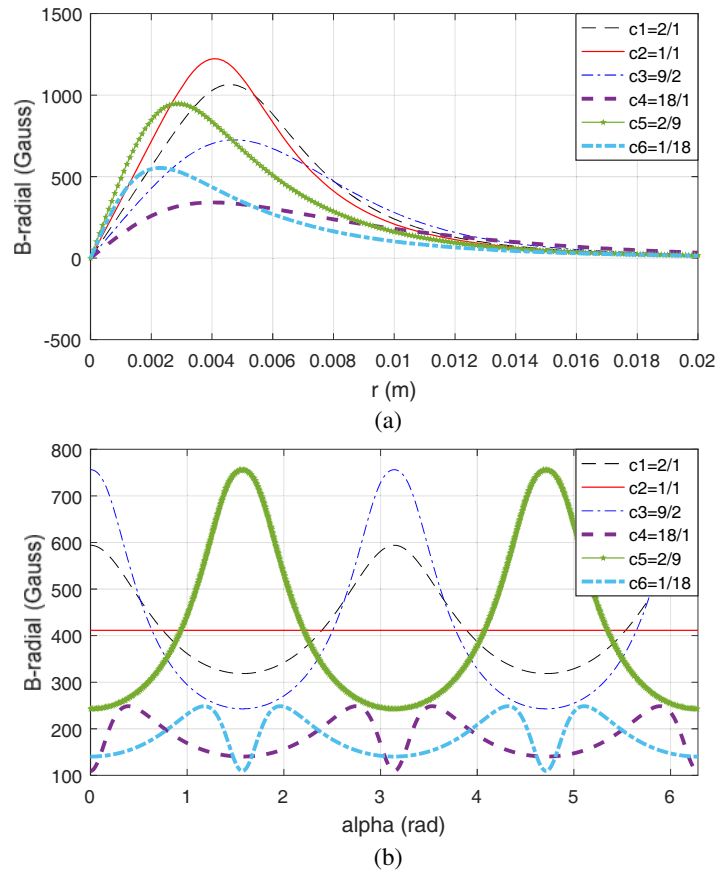


**Figure 9.** Distribution of the radial component (the thickness of the used cylinder is  $h = 5$  mm; the magnetic remanence  $J = 1$  T; the axial coordinate of the computed profile is  $z = 7$  mm): (a) plot along the radial distance  $r$  in the interval  $[0 \text{ mm}, 20 \text{ mm}]$  with azimuthal angle  $\alpha = \pi/6$ ; (b) plot along the azimuthal angle  $\alpha$  (alpha) with radial distance  $r = 8$  mm.

341.4 Gauss at  $r = 3.9$  mm for  $c4$ , 947 Gauss at  $r = 2.8$  mm for  $c5$ , and 553.3 Gauss at  $r = 2.3$  mm for  $c6$ . The value of this component of the circular cylinder ( $c2 = 1/1$ ) is a positive constant (411.7 Gauss) along the azimuthal angle (Table 2). The distribution of this component of an elliptical cylinder along the azimuthal angle is periodical; however, its amplitudes and phases change due to the variations of  $c$ . For the same area, elliptical cylinders with  $c1 = 2/1$ ,  $c3 = 9/2$ , and  $c5 = 2/9$  can produce the periodical magnetic field with larger amplitudes than a circular cylinder. The amplitudes of the periodical distribution (Table 2) are 594.0 Gauss for  $c1$ , 756.2 Gauss for  $c3$ , 248.6 Gauss for  $c4$  and  $c6$ , and 756.2 Gauss for  $c5$ . The variations in magnetic field strength of axial, azimuthal and radial components may be used in novel sensing applications.

## 5. CONCLUSION

In this research, the semi-analytical expressions of three components of the magnetic field created by an elliptical cylinder with axial magnetization in three dimensional space are derived. The magnetic field distribution created by the permanent magnet is analysed. The results of the new expressions are in excellent agreement with those of FEA. These expressions are fast-computed and can be extended to compute the magnetic field created by an arc-shaped elliptical cylinder with axial magnetization which can be used in a novel Halbach array as well as a circular cylinder with the same magnetization direction. The magnetic field distribution of an elliptical cylinder with axial magnetization along the azimuthal angle is periodical whereas a circular cylinder produces a constant value. Along the radial distance, the

axial and radial components of the magnetic field of a circular cylinder can obtain larger values, but eventually drop down over the counterparts of an elliptical cylinder. The azimuthal component of a circular cylinder is zero due to its symmetry whereas an elliptical cylinder produces large amplitudes.

## APPENDIX A. INTEGRATION STEP

This section presents the step integration used when integrating Eqs. (14), (17), and (20). For the purpose of generality, the following step integration is carried out for two key components (Eqs. (A1) and (A2)) in the mentioned equations. The integral variables in these equations are replaced by “ $t$ ” for brevity.

### A.1. Step Integration of $A = \int \frac{tdt}{(t^2 - at + b)^{\frac{3}{2}}}$ with $4b > a^2$

$$A = \int \frac{tdt}{(t^2 - at + b)^{\frac{3}{2}}} = \int \frac{tdt}{\left(\left(t - \frac{a}{2}\right)^2 + \frac{4b - a^2}{2}\right)^{\frac{3}{2}}} = \int \frac{\left(t + \frac{a}{2}\right) dt}{\left(\left(t - \frac{a}{2}\right)^2 + \frac{4b - a^2}{2}\right)^{\frac{3}{2}}} - \int \frac{\frac{a}{2} dt}{\left(\left(t - \frac{a}{2}\right)^2 + \frac{4b - a^2}{2}\right)^{\frac{3}{2}}} \quad (\text{A1})$$

Denote  $u = t - \frac{a}{2}$ , Eq. (A1) becomes

$$A = \int \frac{udu}{\left((u)^2 + \frac{4b - a^2}{2}\right)^{\frac{3}{2}}} - \int \frac{\frac{a}{2} du}{\left((u)^2 + \frac{4b - a^2}{2}\right)^{\frac{3}{2}}} \quad (\text{A2})$$

Integrating the basic integrals of Eq. (A2) based on  $u$  and then returning the variable to  $t$  with some simplifications gives:

$$A = \frac{2(at - 2b)}{(4b - a^2) \sqrt{t(t - a) + b}} + C \quad (\text{A3})$$

Here  $C$  is the integral constant.

### A.2. Step Integration of $B = \int \frac{t^2 dt}{(t^2 - at + b)^{\frac{3}{2}}}$ with $4b > a^2$

$$B = \int \frac{(t^2 - at + b) dt}{(t^2 - at + b)^{\frac{3}{2}}} - \int \frac{at dt}{(t^2 - at + b)^{\frac{3}{2}}} + \int \frac{b dt}{(t^2 - at + b)^{\frac{3}{2}}} \quad (\text{A4})$$

Denote  $u = t - \frac{a}{2}$ , Eq. (A4) becomes

$$B = \int \frac{du}{\sqrt{\left(u\right)^2 + \frac{4b - a^2}{2}}} - aA + \int \frac{b du}{\left(\left(u\right)^2 + \frac{4b - a^2}{2}\right)^{\frac{3}{2}}} \quad (\text{A5})$$

Integrating the basic integrals of Eq. (A5) and applying the result of the above integration, then returning to variable  $t$  with some simplifications produces:

$$B = \ln \left( \left| 2 \left( \sqrt{t(t - a) + b} + t \right) - a \right| \right) - \frac{2t(2b - a^2) + 2ab}{(4b - a^2) \sqrt{t(t - a) + b}} + C \quad (\text{A6})$$

## ACKNOWLEDGMENT

The authors are grateful to the EMWORKS Company for providing the license for the EMS software to conduct the Finite Element Analyses. The authors would like to thank the School of Mechanical Engineering, University of Adelaide, Australia for providing the equipment, facilities and assistance for this research. We are also grateful to Alison-Jane Hunter for her time helping to edit the English.

## REFERENCES

1. Wu, S.-T., J.-Y. Chen, and S.-H. Wu, "A rotary encoder with an eccentrically mounted ring magnet," *IEEE Transactions on Instrumentation and Measurement*, Vol. 63, 1907, 2014.
2. Coey, J. M. D., *Magnetism and Magnetic Materials*, Cambridge University Press, 2009.
3. Furlani, E. P., *Permanent Magnet and Electromechanical Devices: Materials, Analysis and Applications*, Academic Press, 2001.
4. Ravaut, R., G. Lemarquand, V. Lemarquand, and C. Depollier, "Analytical calculation of the magnetic field created by permanent-magnet rings," *IEEE Transactions on Magnetics*, Vol. 44, 1982, 2008.
5. Xu, X. N., D. W. Lu, G. Q. Yuan, Y. S. Han, and X. Jin, "Studies of strong magnetic field produced by permanent magnet array for magnetic refrigeration," *Journal of Applied Physics*, Vol. 95, 6307, 2004.
6. Ravaut, R., G. Lemarquand, V. Lemarquand, and C. Depollier, "The three exact components of the magnetic field created by a radially magnetized tile permanent magnet," *Progress In Electromagnetics Research*, Vol. 88, 307–319, 2008.
7. Jian, L. and K. T. Chau, "Analytical calculation of magnetic field distribution in coaxial magnetic gears," *Progress In Electromagnetics Research*, Vol. 92, 1–16, 2009.
8. Yonnet, J.-P., S. Hemmerlin, E. Rulliere, and G. Lemarquand, "Analytical calculation of permanent magnet couplings," *IEEE Transactions on Magnetics*, Vol. 29, 2932, 1993.
9. McClurg, G. O., "Magnetic field distributions for a sphere and for an ellipsoid," *American Journal of Physics*, Vol. 24, 496, 1956.
10. Rakotoarison, H. L., J. P. Yonnet, and B. Delinchant, "Using Coulombian approach for modeling scalar potential and magnetic field of a permanent magnet with radial polarization," *IEEE Transactions on Magnetics*, Vol. 43, 1261, 2007.
11. Nguyen V. T. and T.-F. Lu, "Analytical expression of the magnetic field created by a permanent magnet with diametrical magnetization," *Progress In Electromagnetics Research C*, Vol. 87, 163, 2018.
12. Ravaut, R. and G. Lemarquand, "Magnetic field produced by a parallelepipedic magnet of various and uniform polarization," *Progress In Electromagnetics Research*, Vol. 98, 207–219, 2009.
13. Nguyen, V. T. and T.-F. Lu, "Modelling of magnetic field distributions of elliptical cylinder permanent magnets with diametrical magnetization," *Journal of Magnetism and Magnetic Materials*, Vol. 491, 2019.
14. Kim, W., M. Kim, and Y. Y. Kim, "Polarization of a permanent magnet to yield specific magnetic field Distribution," *Journal of Applied Physics*, Vol. 104, 064915-1, 2008.
15. Acevedo, M. T. M., V. D. D. Zhabon, and O. Otero, "Analytical study of the magnetic field generated by multipolar magnetic configuration," *Journal of Physics: Conference Series*, Vol. 687, 1, 2016.
16. Karttunen, H., P. Kroger, H. Oja, M. Poutanen, and K. J. Donner, *Fundamental Astronomy*, 507, 5th Edition, Springer, 2007.
17. Hideo, K., *The Design, Manufacture and Application of Non-circular Gears*, 1st Edition, Tokyo, Nikkan Industrial Press, 2001.
18. Bair, B. W., "Tooth profile generation and analysis of crowned elliptical gears," *ASME Journal of Mechanical Design*, Vol. 131, 0745031, 2009.
19. Chen, C. F. and C. B. Tsay, "Computerized tooth profile generation and analysis of characteristics of elliptical gears with circular-arc teeth," *Journal of Materials Processing Technology*, Vol. 148, 226, 2004.
20. Ciarrocchi, M., V. D. Miccoli, M. Alecci, A. Sotgiu, and A. Galante, "Design of an elliptical permanent magnet for surface magnetic resonance imaging," *Measurement Science and Technology*, Vol. 20, 1–4, 2008.

21. Filsoufi, F., R. S. Farivar, L. Aklog, C. A. Anderson, R. H. Chen, S. Lichtenstein, J. Zhang, and D. H. Adams, "Automated distal coronary bypass with a novel magnetic coupler (MVP system)," *The Journal of Thoracic and Cardiovascular Surgery*, Vol. 127, 185, 2004.
22. Takazakura, T., T. Morita, and T. Sugiura, "Dynamical behaviour of noncontact driving cam mechanism using permanent magnets," *International Journal of Applied Electromagnetics and Mechanics*, Vol. 52, 169, 2016.
23. Caciagli, A., R. J. Baars, A. P. Philipse, and B. W. M. Kuipers, "Exact expression for the magnetic field of a finite cylinder with arbitrary uniform magnetization," *Journal of Magnetism and Magnetic Materials*, Vol. 456, 423–432, 2018.
24. Strubecker, K., *Vorlesungenüber Darstellende Geometrie*, 26, Gottingen, Vandenhoeck & Ruprecht, 1967.
25. Bjork, R., "The ideal dimensions of a Halbach cylinder of finite length," *Journal of Applied Physics*, Vol. 109, 013915-1-6, 2011.